Vibrations of a Parametrically Excited MEMS-Structure with Two Masses

Johannes Welte, Horst Ecker

Vienna University of Technology, Institute of Mechanics and Mechatronics, A-1040 Vienna, Austria
(e-mail: horst.ecker@tuwien.ac.at)

Abstract: The impact of time-periodic coefficients, also known as parametric excitation, on the dynamic stability of MEMS-structures is investigated. While single-dof MEMS only exhibit unstable behavior within certain intervals of the parametric excitation frequency, do multi-dof systems also show frequency intervals of enhanced stability. This phenomenon is modeled and studied for a MEMS-structure and some novel results are discussed.

Keywords: Stability, damping, anti-resonance, parametric excitation, MEMS.

1. INTRODUCTION

Microelectromechanical systems (MEMS) are becoming more and more important for all kinds of industrial applications. One of them are filters in communication devices, due to the growing demand for efficient and accurate filtering of signals, see Rhoads et al. (2005). In recent developments single degree of freedom (1-dof) oscillators that are operated at a parametric resonance are employed for such tasks. Typically vibration damping is low in such MEM systems. While parametric excitation (PE) is used so far to take advantage of a parametric resonance, this contribution suggests to also exploit parametric anti-resonances in order to improve the damping behavior of such systems. Modeling aspects of a 2-dof MEM system and some first and novel results are the focus of this paper.

2. SINGLE DEGREE OF FREEDOM MEMS

Figure 1 shows the basic design of a parametrically excited MEMS. Such a system design is well established in the relevant literature, see e.g. Rhoads et al. (2005) , and may be used for chemical sensors or electrical filters.

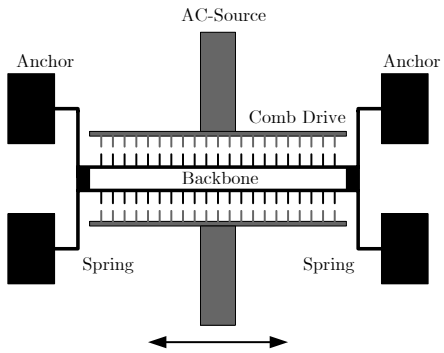

Fig. 1. Basic design of a single degree of freedom MEMS

The main component of the design is the backbone mass. It is connected to elastic beam structures on each side, which act as springs and allow for a translational motion of the oscillator. To generate motion of the system a pair of non-interdigitated comb drives is connected to the backbone mass. By applying an alternating voltage at a certain frequency to the comb drives, the system may start to oscillate at that frequency due to the electrostatic forces generated between the fixed and the free comb.

2.1 Modeling the mechanical 1-dof system

The displacement x of the MEMS can be described by the following differential equation

$$m\ddot{x} + (c_{01} + c_{02})\dot{x} + F_r(x) + F_{es}(x, \omega, t) = 0. \quad (1)$$

For an easier interpretation of the upcoming simulation results it is beneficial to make the differential equation non-dimensional. Therefore, a non-dimensional parametric excitation frequency Ω is introduced. This frequency is related to the actual parametric excitation frequency ω as follows

$$\Omega = \frac{\omega}{\hat{\omega}}, \quad (2)$$

where $\hat{\omega}$ is a characteristic reference frequency. In the present case, given a system with just a single degree of freedom, it is beneficial to use the natural frequency of the linearized system $\hat{\omega}$ as a reference. In order to obtain a scaled system time t, a dimensionless time τ is introduced, which leads to

$$\tau = \hat{\omega}t, \qquad \omega t = \Omega\hat{\omega}t = \Omega\tau. \quad (3)$$

The displacement x of the single backbone mass is rescaled according to

$$z = \frac{x}{x_0}, \quad (4)$$

where x_0 is a scaling parameter of suitable size related to the system's physical dimensions. Carrying out the rescaling, leads to a non-dimensional differential equation of the form

$$z'' + z'(\xi_1 + \xi_2) + z\left[1 + \lambda_1 + \lambda_1 \cos(\Omega\tau)\right] + z^3\left[\chi + \lambda_3 + \lambda_3 \cos(\Omega\tau)\right] = 0, \quad (5)$$

where the new symbols z', z'' and the linear and nonlinear non-dimensional parameters are defined as listed and explained in Table 1.

Definition	Non-dimensional parameter
$z' = \frac{dz}{d\tau}$	Scaled time derivative
$\Omega = \frac{\omega}{\hat{\omega}}$	Non-dimensional excitation frequency
$\xi_1 = \frac{c_{01}}{m\hat{\omega}}$	Scaled damping ratio for c_{01}
$\xi_2 = \frac{c_{02}}{m\hat{\omega}}$	Scaled damping ratio for c_{02}
$\lambda_1 = \frac{r_{1A}V_A^2}{k_{01}^{lin}+k_{02}^{lin}}$	Linear electrostatic excitation amplitude
$\lambda_3 = \frac{x_0^2 r_{3A}V_A^2}{k_{01}^{lin}+k_{02}^{lin}}$	Nonlinear electrostatic excitation coefficient
$\chi = \frac{\left(k_{01}^{nlin}+k_{02}^{nlin}\right)x_0^2}{k_{01}^{lin}+k_{02}^{lin}}$	Nonlinear mechanical stiffness coefficient

Table 1. Non-dimensional parameter definitions adapted from Rhoads et al. (2005)

2.2 Numerical stability investigation

To solve the equation of motion (1) numerical integration in the time domain was used and the resulting vibrations were analyzed in regard of the stability of the present system. The dependency of the system stability on the voltage amplitude V_A is depicted in Fig. 2. Due to the linear electrostatic excitation amplitude λ_1, which is quadratic in V_A, the stability boundaries are curved. The solid line which is denoted $D = 0$ holds for the undamped system $\xi_1 = \xi_2 = 0$.

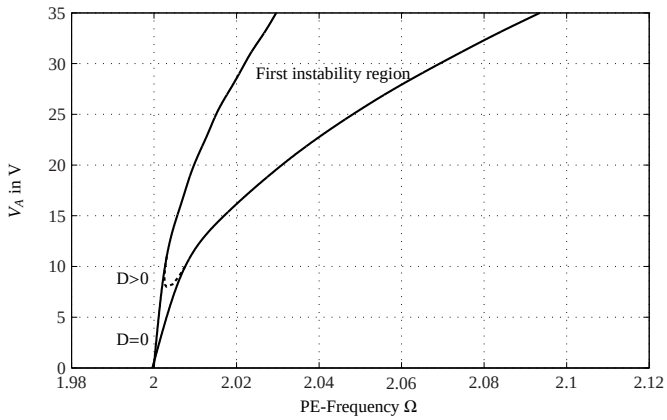

Fig. 2. First region of parametric instability of a 1-dof system

3. MEMS WITH TWO DEGREES OF FREEDOM

Based on the investigations of the single degree of freedom system, a parametrically excited oscillator with two degrees of freedom is now investigated. First, a mechanical model is developed and the governing differential equations are derived. Then the model is analyzed with regard to parametric resonances, especially so-called anti-resonances, see Tondl (1998). To identify the various regions of stability and instability the monodromy matrix of the system is calculated numerically, since its eigenvalues determine the stability of the system. Finally, a parameter study is carried out to individually optimize the linear system parameters, in order to obtain a maximized effect of the anti-resonance phenomenon.
The oscillator design aimed for with two degrees of freedom is achieved by combining two oscillators with a system design similar to the one shown in Fig. 1. Instead of the two fixed anchors on the right hand side, another set of springs connected to a second backbone mass is attached to the original design. An additional set of non-interdigitated comb drives is connected as well to the newly introduced backbone mass. The expansion of the single degree of freedom system design may result in an oscillator with a basic layout shown in Fig. 3.

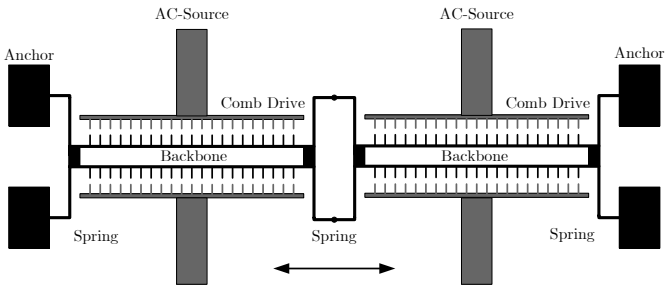

Fig. 3. Basic design of a MEMS with two degrees of freedom

3.1 Modeling the 2-dof mechanical system

In principle the system is an oscillating mechanical system with two degrees of freedom $\mathbf{x} = [x_1, x_2]^T$ that can be described by

$$\mathbf{M}\ddot{\mathbf{x}} + \mathbf{C}\dot{\mathbf{x}} + \mathbf{F}_r(\mathbf{x}) + \mathbf{F}_{es}(\mathbf{x}, \omega, t) = 0, \tag{6}$$

where the electrostatic restoring forces are represented by the matrix F_{es} and the mechanical restoring forces provided by the springs are represented by the matrix F_r. The mass matrix is denoted $\mathbf{M}$ and the damping matrix $\mathbf{C}$,

$$\mathbf{M} = \begin{bmatrix} m_1 & 0 \\ 0 & m_2 \end{bmatrix}, \quad \mathbf{C} = \begin{bmatrix} c_{01} + c_{12} & -c_{12} \\ -c_{12} & c_{02} + c_{12} \end{bmatrix}. \tag{7}$$

Fitting the nonlinear mechanical restoring forces by cubic functions of displacement, results in the following stiffness matrix $\mathbf{F_r}$

$$\mathbf{F}_r(\mathbf{x}) = \begin{bmatrix} F_{r1}(x_1, x_2) \\ F_{r2}(x_1, x_2) \end{bmatrix} \tag{8}$$

$$\mathbf{F}_r(\mathbf{x}) = \mathbf{F}_r^{lin}(\mathbf{x}) + \mathbf{F}_r^{nlin}(\mathbf{x}^3)$$

$$\mathbf{F}_r(\mathbf{x}) = \begin{bmatrix} k_{01}^{lin} + k_{12}^{lin} & -k_{12}^{lin} \\ -k_{12}^{lin} & k_{02}^{lin} + k_{12}^{lin} \end{bmatrix} \mathbf{x} +$$

$$\begin{bmatrix} (k_{01}^{nlin} + k_{12}^{nlin})x_1^2 + 3k_{12}^{nlin}x_2^2 & -3k_{12}^{nlin}x_1^2 - k_{12}^{nlin}x_2^2 \\ -k_{12}^{nlin}x_1^2 - 3k_{12}^{nlin}x_2^2 & 3k_{12}^{nlin}x_1^2 + (k_{02}^{nlin} + k_{12}^{nlin})x_2^2 \end{bmatrix} \mathbf{x}$$

As the electrostatic restoring forces are depending on the displacement $\mathbf{x}$ as well as on time t, they are represented by a time dependent stiffness matrix $\mathbf{F_{es}}$. The time-periodicity of that matrix introduces parametric excitation to the system.

$$\mathbf{F}_{es}(\mathbf{x},t) = \begin{bmatrix} F_{es1}(x_1,t) \\ F_{es2}(x_2,t) \end{bmatrix} \tag{9}$$
$$\mathbf{F}_{es}(\mathbf{x},t) = \mathbf{F}_{es}^{lin}(\mathbf{x},t) + \mathbf{F}_{es}^{nlin}(\mathbf{x}^3,t)$$
$$\mathbf{F}_{es}(\mathbf{x},t) = \begin{bmatrix} r_{1A}V_A^2(1+\cos(\omega t)) & 0 \\ 0 & r_{1A}V_A^2(1+\cos(\omega t)) \end{bmatrix} \mathbf{x} + \begin{bmatrix} r_{3A}V_A^2 x_1^2(1+\cos(\omega t)) & 0 \\ 0 & r_{3A}V_A^2 x_2^2(1+\cos(\omega t)) \end{bmatrix} \mathbf{x}$$

For an easier interpretation of the upcoming simulation results and efficient numerical treatment, the nonlinear differential equation (6) is scaled. Therefore, a non-dimensional parametric excitation frequency Ω is introduced the same way as in Eq. (2), with the characteristic reference frequency $\hat{\omega}$ being defined as the natural frequency of a linearized subsystem. This subsystem can be derived from the original system as shown in Fig. 3 by setting all spring (and damping) constants to zero, except for k_{01}^{lin}. The remaining subsystem consist only of mass m_1 and the linear mechanical spring k_{01}^{lin}. The natural frequency of that subsystem is known to be

$$\hat{\omega} = \sqrt{\frac{k_{01}^{lin}}{m_1}}. \tag{10}$$

To obtain a scaled system time, a dimensionless time τ is introduced by multiplying time t with the reference frequency $\hat{\omega}$ according to Eq. (3). The displacements x_1 and x_2 of the oscillator are rescaled using a convenient scaling parameter x_0

$$z_1 = \frac{x_1}{x_0}, \qquad z_2 = \frac{x_2}{x_0}. \tag{11}$$

Carrying out the rescaling substitutions leads to a non-dimensional differential equation of the form

$$\mathbf{z}'' + \hat{\mathbf{C}}\mathbf{z}' + \hat{\mathbf{F}}_{es}(\mathbf{z}) + \cos(\Omega\tau)\hat{\mathbf{P}}_C(\mathbf{z}) + \hat{\mathbf{F}}_r(\mathbf{z}) = 0, \tag{12}$$

where the rescaled damping matrix is denoted $\hat{\mathbf{C}}$ and the vector of scaled deflections is $\mathbf{z}$,

$$\hat{\mathbf{C}} = \begin{bmatrix} \xi_{01}+\xi_{12} & -\xi_{12} \\ -\gamma\xi_{12} & \gamma(\xi_{02}+\xi_{12}) \end{bmatrix}, \qquad \mathbf{z} = \begin{bmatrix} z_1 \\ z_2 \end{bmatrix}. \tag{13}$$

The rescaled mechanical and electrostatic stiffness matrices are denoted $\hat{\mathbf{F}}_r$ and $\hat{\mathbf{F}}_{es}$, respectively. In addition to both stiffness matrices a matrix $\hat{\mathbf{P}}_C$ is introduced to clearly point out the parametric excitation mechanism. The definitions of these three matrices are listed below, whereas the newly introduced non-dimensional parameters are defined as stated in Table 2.

$$\hat{\mathbf{F}}_r(\mathbf{z}) = \hat{\mathbf{F}}_r^{lin}(\mathbf{z}) + \hat{\mathbf{F}}_r^{nlin}(\mathbf{z}^3) \tag{14}$$
$$\hat{\mathbf{F}}_r(\mathbf{z}) = \begin{bmatrix} 1+\beta_{12} & -\beta_{12} \\ -\gamma\beta_{12} & \gamma(\beta_{02}+\beta_{12}) \end{bmatrix} + \begin{bmatrix} (\chi_{01}+\chi_{12})z_1^2 + 3\chi_{12}z_2^2 & -3\chi_{12}z_1^2 - \chi_{12}z_2^2 \\ -\gamma\chi_{12}z_1^2 - 3\gamma\chi_{12}z_2^2 & 3\gamma\chi_{12}z_1^2 + \gamma z_2^2(\chi_{02}+\chi_{12}) \end{bmatrix} \mathbf{z}$$

$$\hat{\mathbf{F}}_{es}(\mathbf{z}) = \hat{\mathbf{F}}_{es}^{lin}(\mathbf{z}) + \hat{\mathbf{F}}_{es}^{nlin}(\mathbf{z}^3) \tag{15}$$
$$\hat{\mathbf{F}}_{es}(\mathbf{z}) = \begin{bmatrix} \lambda_1 & 0 \\ 0 & \gamma\lambda_1 \end{bmatrix} \mathbf{z} + \begin{bmatrix} \lambda_3 z_1^2 & 0 \\ 0 & \gamma\lambda_3 z_2^2 \end{bmatrix} \mathbf{z}$$

$$\hat{\mathbf{P}}_C(\mathbf{z}) = \hat{\mathbf{P}}_C^{lin}(\mathbf{z}) + \hat{\mathbf{P}}_C^{nlin}(\mathbf{z}^3) \tag{16}$$
$$\hat{\mathbf{P}}_C(\mathbf{z}) = \begin{bmatrix} \lambda_1 & 0 \\ 0 & \gamma\lambda_1 \end{bmatrix} \mathbf{z} + \begin{bmatrix} \lambda_3 z_1^2 & 0 \\ 0 & \gamma\lambda_3 z_2^2 \end{bmatrix} \mathbf{z}$$

Definition	Non-dimensional parameter
$z'_{1,2} = \frac{dz_{1,2}}{d\tau}$	Scaled time derivative
$\Omega = \frac{\omega}{\hat{\omega}}$	Non-dimensional excitation frequency
$\gamma = \frac{m_1}{m_2}$	Mass ratio
$\xi_{01} = \frac{c_{01}}{m_1\hat{\omega}}$	Scaled damping ratio for c_{01}
$\xi_{12} = \frac{c_{12}}{m_1\hat{\omega}}$	Scaled damping ratio for c_{12}
$\xi_{02} = \frac{c_{02}}{m_1\hat{\omega}}$	Scaled damping ratio for c_{02}
$\lambda_1 = \frac{r_{1A}V_A^2}{k_{01}^{lin}}$	Linear electrostatic excitation amplitude
$\lambda_3 = \frac{x_0^2 r_{3A}V_A^2}{k_{01}^{lin}}$	Nonlinear electrostatic excitation coefficient
$\beta_{12} = \frac{k_{12}^{lin}}{k_{01}^{lin}}$	Linear mechanical stiffness quotient
$\beta_{02} = \frac{k_{02}^{lin}}{k_{01}^{lin}}$	Linear mechanical stiffness quotient
$\chi_{01} = \frac{k_{01}^{nlin}x_0^2}{k_{01}^{lin}}$	Nonlinear mechanical stiffness coefficient
$\chi_{12} = \frac{k_{12}^{nlin}x_0^2}{k_{01}^{lin}}$	Nonlinear mechanical stiffness coefficient
$\chi_{02} = \frac{k_{02}^{nlin}x_0^2}{k_{01}^{lin}}$	Nonlinear mechanical stiffness coefficient

Table 2. Non-dimensional parameter definitions 2-dof model adapted from Rhoads et al. (2005)

3.2 System parameters

To obtain feasible system parameters, the first step is to define the physical dimensions of the MEMS shown in Fig. 3. On the basis of similar systems described in Madou (2012) the length of the two backbones is set to 400 µm with a width of 20 µm. The folded beams are defined to be 420 µm long with a defined length of the folded part of 20 µm and a width of 2 µm. The thickness of the whole design is set to 12 µm. Using finite element analysis, the mechanical stiffness coefficients are calculated. The system masses originate from the perforated backbone structures. Mass m_2 is chosen to be two times bigger than m_1 in order to obtain a well pronounced anti-resonance phenomenon. The damping coefficients are taken from Rhoads et al. (2005), whereas the electrostatic stiffness coefficients are taken from a numerical characterization of a comb drive carried out in Zhang et al. (2002). Table 3 summarizes the system parameters.

3.3 Numerical stability investigation

In order to know the primary parametric resonances and the combination resonances before applying numerical

Parameter	Value	Units
m_1	1.22×10^{-10}	kg
m_2	2.44×10^{-10}	kg
c_{01}	1.94×10^{-8}	Ns/m
c_{12}	3.88×10^{-8}	Ns/m
c_{02}	1.94×10^{-8}	Ns/m
k_{01}^{lin}	3.505	µN/µm
k_{12}^{lin}	1.753	µN/µm
k_{02}^{lin}	3.505	µN/µm
k_{01}^{nlin}	0.018	µN/µm^3
k_{12}^{nlin}	0.009	µN/µm^3
k_{02}^{nlin}	0.018	µN/µm^3
r_{1A}	3.65×10^{-4}	µN/V^{2}µm
r_{3A}	-1.6×10^{-5}	µN/V^{2}µm^3

Table 3. Parameter values for a two degrees of freedom MEMS

simulation, a modal analysis is carried out on the undamped linear time-invariant system. For this, the rescaled damping matrix $\hat{\mathbf{C}}$ and the coefficient matrix $\hat{\mathbf{P}}_C^{lin}$ of the parametric stiffness variation, as well as the nonlinear stiffness matrices, are not considered. The natural frequencies of the system are obtained from the modal analysis can be calculated from the abbreviated version of system Eq. (12)

$$\Omega_1 = \min\left(\mathrm{eig}\left(\hat{\mathbf{F}}_{es}^{lin} + \hat{\mathbf{F}}_r^{lin}\right)\right), \tag{17}$$
$$\Omega_2 = \max\left(\mathrm{eig}\left(\hat{\mathbf{F}}_{es}^{lin} + \hat{\mathbf{F}}_r^{lin}\right)\right).$$

Due to the rescaling of the differential equations, the obtained natural frequencies are dimensionless. Table 4 summarizes the obtained first primary and combination resonances according to Eq. (18), see Cartmell (1990), for the case where $n = 1$.

$$\Omega = \frac{2\omega_j}{n}, \qquad (n = 1, 2, 3, \ldots) \tag{18}$$
$$\Omega = \frac{\omega_i \pm \omega_j}{n}, \qquad (i, j = 1, \ldots, k)$$

Description	Parameter	Value
Natural frequency	Ω_1	0.8256
Natural frequency	Ω_2	1.3266
Primary resonance	$2\Omega_1$	1.6512
Primary resonance	$2\Omega_2$	2.6532
Combination resonance	$\Omega_1 + \Omega_2$	2.1522
Combination anti-resonance	$\Omega_2 - \Omega_1$	0.501

Table 4. Dimensionless primary and combination resonances of the 2-dof MEMS

For the linearized time-periodic MEMS structure, the stability can be investigated by examining the eigenvalues of the Monodromy matrix Φ, see Ecker (2005). If $\max(|\mathrm{eig}(\Phi)|) > 1$ holds for the largest eigenvalue, then the system is unstable. Figure 4 shows a stability chart where this eigenvalue is plotted as a function of the non-dimensional parametric excitation (PE) frequency Ω and the amplitude V_A of the input voltage.

Areas of the surface that raise above the plane at level 1 indicate an unstable system. The stability chart confirms the theoretical parametric resonance conditions Eq. (18) and exhibits parametric resonances at $2\Omega_1$ and $2\Omega_2$ and at the first combination resonance $\Omega_1 + \Omega_2$. Also the anti-resonance phenomenon at $\Omega = \Omega_2 - \Omega_1 = 0.501$ is found,

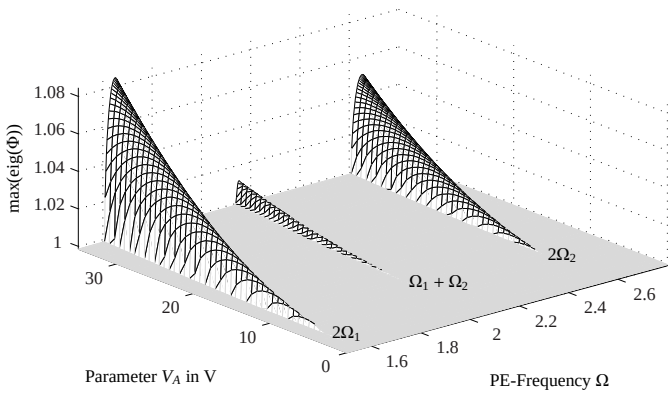

Fig. 4. Stability investigation for PE-Frequency Ω and input voltage V_A. Parameter values as in Table 3

but is located outside the plotted parameter range. In anticipating further results, a comparable plot can be seen in Fig. 8. From that figure one can see that the maxima of the eigenvalues decrease in the region near the parametric anti-resonance $\Omega_2 - \Omega_1$, indicating that the system not only operates in a stable condition, but also enhanced vibration damping can be expected, see Ecker (2005), and Tondl (1998).

3.4 Parameter study

To obtain an oscillator design where the anti-resonance phenomenon is pronounced and enhanced damping is maximized, a parameter study is carried out, see also Welte (2012). By varying each of the linear system parameters in individual studies, they can be optimized with respect to the first anti-resonance occurring at $\Omega = \Omega_2 - \Omega_1$. Figures 5 to 8 exemplarily show the results of the parameter study for a certain set of the linear system parameters. A summary of the optimized system parameters is given in Table 5.

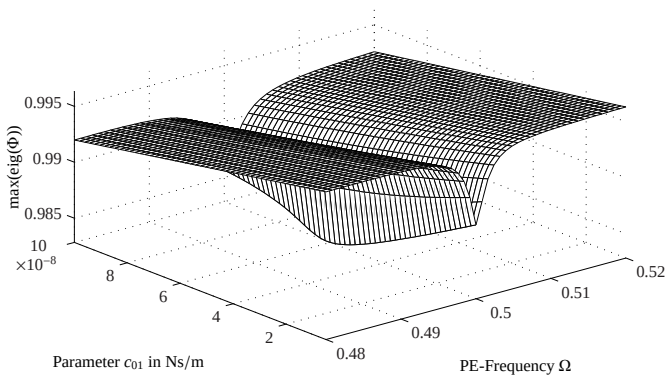

Fig. 5. Simulation study for PE-Frequency Ω and damping coefficient c_{01}

To visualize the effect of the parameter optimization, the shape of the stability threshold near the first anti-resonance at $\Omega = \Omega_2 - \Omega_1$ is analyzed with two different sets of parameters. Figure 9 a) shows a stability chart using the non-optimized (default) linear system parameters stated in Table 3. In comparison to that, Fig. 9 b) shows a stability chart using the optimized linear system

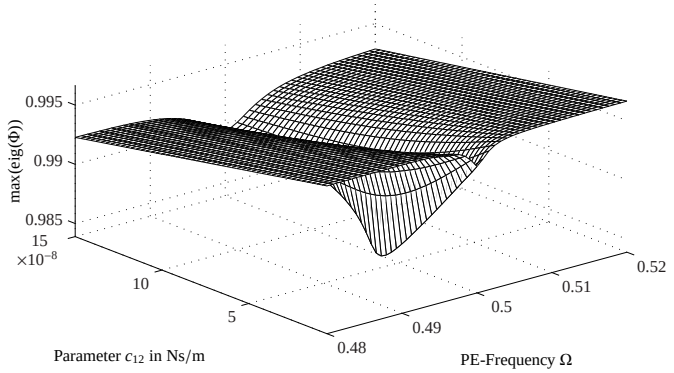

Fig. 6. Simulation study for PE-Frequency Ω and damping coefficient c_{12}

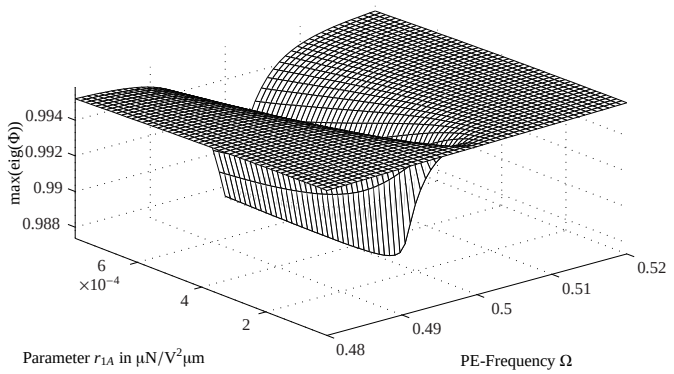

Fig. 7. Simulation study for PE-Frequency Ω and linear electrostatic coefficient r_{1A}

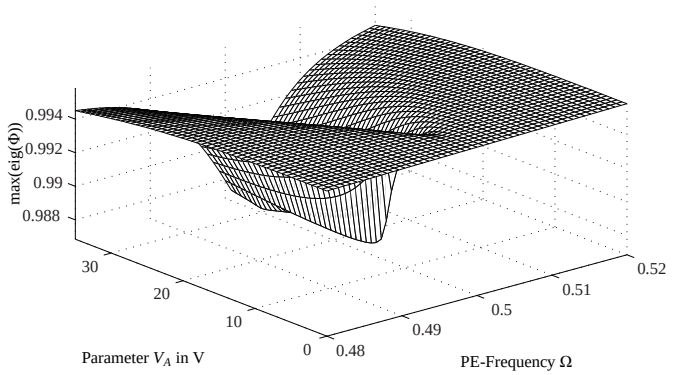

Fig. 8. Simulation study for PE-Frequency Ω and input voltage V_A

parameters, obtained from the parameter study and listed in Table 5.

A comparison of both stability charts shows that the set of optimized parameters leads to a more pronounced occurrence of the first anti-resonance than the set of default parameters. As the magnitude of the maximum eigenvalue does not directly reflect the oscillation amplitudes, both stability charts are just an indication for the damping behavior at and near the anti-resonance. To verify that result, the system is analyzed in the time domain, see the results in Fig. 10. Due to the decrease of the oscillation amplitudes with growing time, both displacement signals confirm a stable system behavior as expected when oper-

Parameter	Value	Units
m_1	1.45×10^{-10}	kg
m_2	2.9×10^{-10}	kg
c_{01}	6.0×10^{-8}	Ns/m
c_{12}	6.0×10^{-8}	Ns/m
c_{02}	2.0×10^{-8}	Ns/m
k_{01}^{lin}	2.3	μN/μm
k_{12}^{lin}	1.4	μN/μm
k_{02}^{lin}	6.0	μN/μm
r_{1A}	3.8×10^{-4}	μN/V²μm
V_A	16	V

Table 5. Optimized parameter values for the linearized 2-dof MEMS

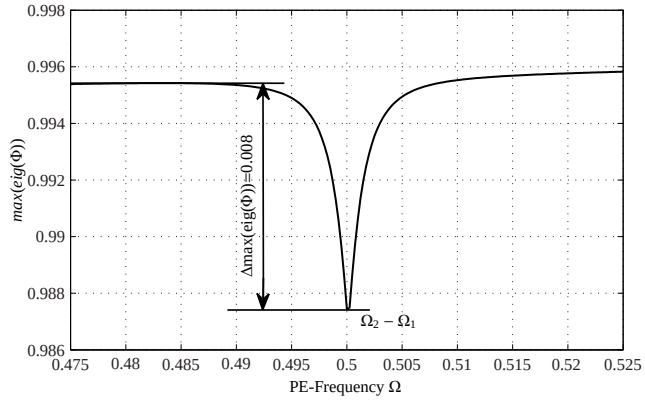

a) Stability investigation near the first anti-resonance at $\Omega = \Omega_2 - \Omega_1$ and $V_A = 16$V with default parameters taken from Table 3

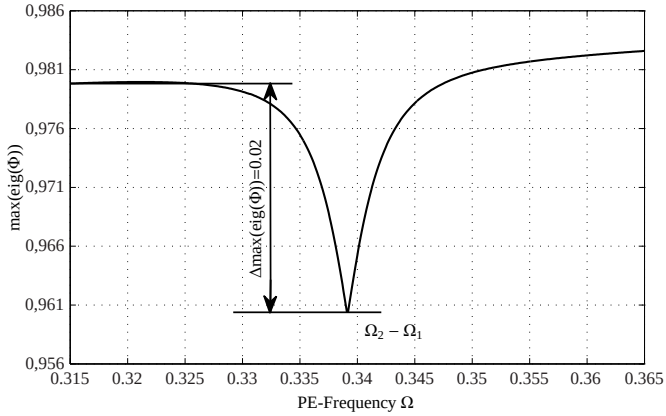

b) Stability investigation near the first anti-resonance at $\Omega = \Omega_2 - \Omega_1$ and $V_A = 16$V with optimized parameters taken from Table 5

Fig. 9. Stability threshold near the first anti-resonance frequency for different sets of parameters

ating the oscillatory system near the first anti-resonance frequency. It can be seen also that the exponential decrease of the amplitudes z_1 and z_2 in Fig. 10 b) is more pronounced than in Fig. a). This fact acknowledges the premise that the set of optimized parameters leads to a stronger occurrence of the anti-resonance phenomenon. The displacement signals prove that an enlarged stability area near an anti-resonance frequency implies enhanced vibration damping.

Figure 11 shows the displacements z_1 and z_2 at the first anti-resonance $\Omega = \Omega_2 - \Omega_1$ for the *nonlinear* system.

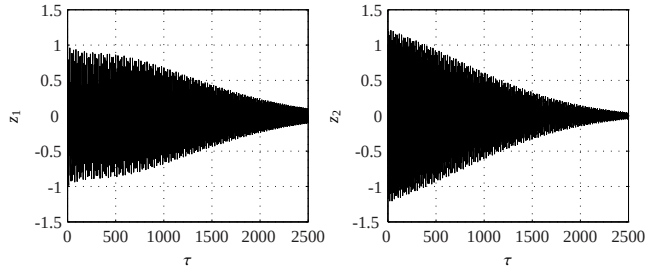

(a) Displacements z_1,z_2 of the linearized system at $\Omega = \Omega_2 - \Omega_1$ with $V_A = 16$V and default parameters taken from Table 3

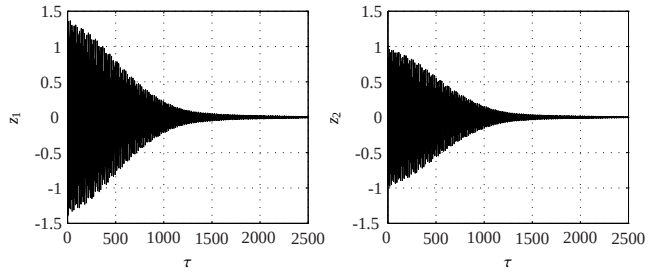

(b) Displacements z_1,z_2 of the linearized system at $\Omega = \Omega_2 - \Omega_1$ with $V_A = 16$V and optimized parameters taken from Table 5

Fig. 10. Displacements z_1,z_2 at $\Omega = \Omega_2 - \Omega_1$ with different sets of parameters

Comparing that plot to the one shown in Fig. 10 a), leads to the conclusion that the consideration of the nonlinearities has no remarkable effect on the resulting vibrations. The reason for this is that, first of all, the nonlinear mechanical and electrostatic stiffness coefficients are much smaller than their linear counterparts and, second, also the deflections get smaller and smaller. Thus, it can be concluded that the nonlinearities have no negative consequences for the exploitation of the parameter anti-resonance phenomenon and hence the performed linear stability analysis and the parameter studies are appropriate methods of investigation.

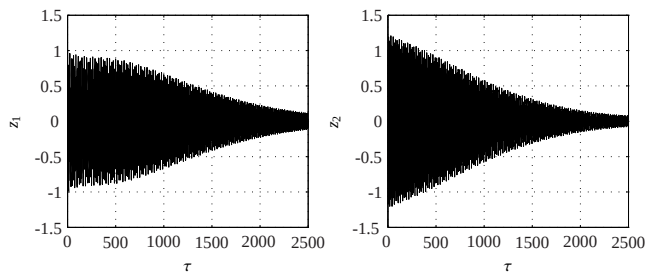

Fig. 11. Displacements z_1,z_2 at $\Omega = \Omega_2 - \Omega_1$ with $V_A = 16$V and default parameters taken from Table 3

4. OPTIMIZED MEMS DESIGN WITH RESPECT TO THE PARAMETRIC ANTI-RESONANCE PHENOMENON

By transforming the optimized linear system parameters into an oscillator design, one obtains the basic layout shown in Fig. 12. To achieve stiffness parameters which are independent of the direction of deflection, the two outer spring structures are replaced by two straight beams in a fixed-fixed configuration, compared to the original folded design shown in Fig. 1. Finite element analyses have been used to obtain the beam lengths needed to correspond with the optimized stiffness coefficients. Table 6 summarizes the physical dimensions of the structure as depicted in Fig. 12.

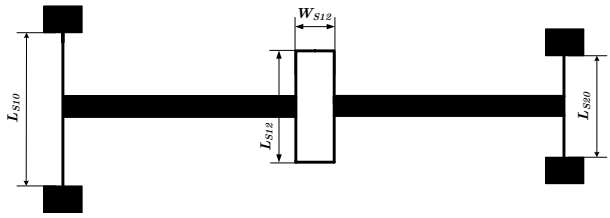

Fig. 12. Basic MEMS layout for maximum anti-resonance

Parameter	Value	Units
Width of springs	2	µm
Width of backbone	20	µm
Depth	12	µm
L_{S10}	490	µm
L_{S12}	400	µm
L_{S20}	360	µm
W_{S12}	40	µm

Table 6. Dimensions of the 2-dof MEMS optimized for enhanced damping at parametric anti-resonance frequency

ACKNOWLEDGEMENTS

The authors would like to thank Prof. Dr. Ulrich Schmidt, Vienna Univ. of Technology, for the fruitful discussions on the design of MEMS.

REFERENCES

Cartmell, M. (1990). *Introduction to Linear, Parametric and Nonlinear Vibrations.* Chapman and Hall, London.

Ecker, H. (2005). *Suppression of Self-excited Vibrations in Mechanical Systems by Parametric Stiffness Excitation.* Argesim/ASIM, Vienna.

Madou, J.M. (2012). *Fundamentals of Microfabrication and Nanotechnology.* Francis&Taylor, Boca Raton.

Rhoads, J., Shaw, S.W., Turner, K., and Baskaran, R. (2005). Tunable microelectromechanical filters that exploit parametric resonance. *Journal of Vibration and Acoustics*, 127, 423–432.

Tondl, A. (1998). To the problem of quenching self-excited vibrations. *Acta Technica CSAV*, 43, 109–116.

Welte, J. (2012). *Parametric Excitation in Micro-Electro-Mechanical Systems.* Master Thesis, TU-Vienna, Vienna.

Zhang, W., Baskaran, R., and Turner, K. (2002). Effect of cubic nonlinearity on auto-parametrically amplified resonant mems mass sensor. *Sensors and Actuators A: Physical*, 102, 139–150.